Hexagonal liquid crystal lens array for 3D endoscopy

Amir Hassanfiroozi,[1] Yi-Pai Huang,[1*] Bahram Javidi[2] and Han-Ping D.Shieh[1]

[1]*Department of Photonics and the Institute of Electro-Optical Engineering/Display Institute, National Chiao Tung University, 30010 Hsinchu, Taiwan*

[2]*Electrical and Computer Engineering Department, University of Connecticut, Storrs, CT 06269-4157, USA*

**boundshuang@mail.nctu.edu.tw*

Abstract: A liquid crystal lens array with a hexagonal arrangement is investigated experimentally. The uniqueness of this study exists in the fact that using convex-ring electrode provides a smooth and controllable applied potential profile across the aperture to manage the phase profile. We observed considerable differences between flat electrode and convex-ring electrode; in particular the lens focal length is variable in a wider range from 2.5cm to infinity. This study presents several noteworthy characteristics such as low driving voltage; 30 μm cell gap and the lens is electrically switchable between 2D/3D modes. We demonstrate a hexagonal LC-lens array for capturing 3D images by using single sensor using integral imaging.

OCIS codes: (170.2150) Endoscopic imaging; (230.3720) Liquid-crystal devices.

References and links

1. S. Sato, "Liquid-crystal lens-cells with variable focal length," Jpn. J. Appl. Phys. **18**(9), 1679–1684 (1979).
2. H. Ren and S.-T. Wu, "Adaptive liquid crystal lens with large focal length tunability," Opt. Express **14**(23), 11292–11298 (2006).
3. Y.-P. Huang, H.-P. D. Shieh, and S.-T. Wu, "Applications of multidirectional asymmetrical microlens-array light-control films on reflective liquid-crystal displays for image quality enhancement," Appl. Opt. **43**(18), 3656–3663 (2004).
4. O. Pishnyak, S. Sato, and O. D. Lavrentovich, "Electrically tunable lens based on a dual-frequency nematic liquid crystal," Appl. Opt. **45**(19), 4576–4582 (2006).
5. Z. He, T. Nose, and S. Sato, "Optical Performance of Liquid Crystal Cells with Asymmetric Slit-Patterned Electrodes in Various Applied Field Configurations," Jpn. J. Appl. Phys. **33**(1), 1091–1095 (1994).
6. M. Ye, B. Wang, and S. Sato, "Liquid-crystal lens with a focal length that is variable in a wide range," Appl. Opt. **43**(35), 6407–6412 (2004).
7. H. Ren, S. Xu, Y. Liu, and S.-T. Wu, "Switchable focus using a polymeric lenticular microlens array and a polarization rotator," Opt. Express **21**(7), 7916–7925 (2013).
8. M. Ye, B. Wang, M. Uchida, S. Yanase, S. Takahashi, and S. Sato, "Focus tuning by liquid crystal lens in imaging system," Appl. Opt. **51**(31), 7630–7635 (2012).
9. R. Zhu, S. Xu, Q. Hong, S.-T. Wu, C. Lee, C.-M. Yang, C.-C. Lo, and A. Lien, "Polymeric-lens-embedded 2D/3D switchable display with dramatically reduced crosstalk," Appl. Opt. **53**(7), 1388–1395 (2014).
10. A. Hassanfiroozi, T.-H. Jen, Y.-P. Huang, and H.-P. D. Shieh, "Liquid crystal lens array for a 3D endoscope," Biomedical Optics & Medical Imaging, SPIE Newsroom (2014). DOI: 10.1117/2.1201405.005419.
11. M. Singer, J. Endres, A. Yetasook, W. Halabi, I. Voskresensky, M. J. Stamos, and R. Clements, "Evaluation of 3-D laparoscopy to complete surgical skills tasks," Surgical Endoscopy: 2013 Sci. Sess. Soc. Amer. Gastrointest. Endoscop. Surgeons **27**(S304–S503), P520 (2013).
12. Y.-P. Huang, C.-W. Chen, M. Cho, and B. Javidi, "Liquid crystal lens for axially distributed three-dimensional sensing," Proc. SPIE **8738**, 873804 (2013).
13. Y.-C. Chang, T.-H. Jen, C.-H. Ting, and Y.-P. Huang, "High-resistance liquid-crystal lens array for rotatable 2D/3D autostereoscopic display," Opt. Express **22**(3), 2714–2724 (2014).
14. Y. Yi-Pai Huang, C.-W. Chen, and Y.-C. Huang, "Superzone Fresnel liquid crystal lens for temporal scanning auto-stereoscopic display," J. Display Technol. **8**(11), 650–655 (2012).
15. Y.-P. Huang, L.-Y. Liao, and C.-W. Chen, "2D/3D switchable autostereoscopic display with multi-electrically driven liquid crystal (MeD-LC) lenses," J. Soc. Inf. Disp. **18**(9), 642–646 (2010).
16. M. Kawamura, E. Yumoto, and S. Ishikuro, "Three-dimensional imaging system by using a liquid crystal lens," Proc. Int'l Symp. Optomechatron. Technol. **2**, 1–6, (2012).

#228317 - $15.00 USD Received 20 Nov 2014; revised 9 Jan 2015; accepted 9 Jan 2015; published 15 Jan 2015

17. L. Li, D. Bryant, T. Van Heugten, and P. J. Bos, "Near-diffraction-limited and low-haze electro-optical tunable liquid crystal lens with floating electrodes," Opt. Express **21**(7), 8371–8381 (2013).
18. H.-C. Lin and Y.-H. Lin, "An electrically tunable-focusing liquid crystal lens with a low voltage and simple electrodes," Opt. Express **20**(3), 2045–2052 (2012).
19. C. J. Hsu and C. R. Sheu, "Using photopolymerization to achieve tunable liquid crystal lenses with coaxial bifocals," Opt. Express **20**(4), 4738–4746 (2012).
20. P. C.-P. Chao, Y.-Y. Kao, and C.-J. Hsu, "A new negative liquid crystal lens with multiple ring electrodes in unequal widths," IEEE Photon. J. **4**(1), 250–266 (2012).
21. C.-T. Hsieh, Y.-F. Hsu, C.-W. Chung, M.-F. Chen, W.-C. Su, and C.-Y. Huang, "Distortion aberration correction device fabricated with liquid crystal lens array," Opt. Express **21**(2), 1937–1943 (2013).
22. G. Shibuya, N. Okuzawa, and M. Hayashi, "New application of liquid crystal lens of active polarized filter for micro camera," Opt. Express **20**(25), 27520–27529 (2012).
23. H. Milton, P. Brimicombe, P. Morgan, H. Gleeson, and J. Clamp, "Optimization of refractive liquid crystal lenses using an efficient multigrid simulation," Opt. Express **20**(10), 11159–11165 (2012).
24. Y. C. Chen, L. Y. Liao, Y. P. Huang, and H. P. Shieh, "Extremely-fast focusing gradient driven liquid crystal lens driven by ultra-low operating voltages," International Display Manufacturing Conference, PS-028, (2011).
25. C. W. Chen, Y. P. Huang, and P. C. Chen, "Dual direction overdriving method for fast switching liquid crystal lens on 2D/3D switchable auto-stereoscopic display," IEEE J. Displ. Technol. **8**(10), 559–561 (2012).
26. K. C. Heo, S. H. Yu, J. H. Kwon, and J. S. Gwag, "Thermally tunable-focus lenticular lens using liquid crystal," Appl. Opt. **52**(35), 8460–8464 (2013).
27. M. Xu, H. Ren, C. Nah, S. H. Lee, and Y. Liu, "Liquid crystal microlenticular array assembled by a fringing field," J. Appl. Phys. **111**(6), 063104 (2012).
28. D. Liang and Q.-H. Wang, "Thermally tunable-focus lenticular lens using liquid crystal," J. Display Technol. **9**(10), 814–818 (2013).
29. S. Xu, H. Ren, and S.-T. Wu, "Adaptive liquid lens actuated by liquid crystal pistons," Opt. Express **20**(27), 28518–28523 (2012).
30. H.-S. Chen and Y.-H. Lin, "An endoscopic system adopting a liquid crystal lens with an electrically tunable depth-of-field," Opt. Express **21**(15), 18079–18088 (2013).
31. S.-J. Hwang, Y.-X. Liu, and G. A. Porter, "Improvement of performance of liquid crystal microlens with polymer surface modification," Opt. Express **22**(4), 4620–4627 (2014).
32. H.-C. Lin, M.-S. Chen, and Y.-H. Lin, "A review of electrically tunable focusing liquid crystal lenses," Transactions on Electrical and Electronic Materials **12**(6), 234–240 (2011).
33. K. W. Ian, M. Exarchos, and M. Missous, "A novel low temperature soft reflow process for the fabrication of deep-submicron (<0.35 μm) T-gate pseudomorphic high electron mobility transistor structures," Nanotechnology **24**(5), 055202 (2013).
34. F. M. Pargon, "Atomic force microscopy study of photoresist sidewall smoothing and line edge roughness transfer during gate patterning," J. Micro/Nanolith. MEMS MOEMS. **12**(4), 041308. doi:10.1117/1.JMM.12.4.041308 (2013).
35. C. M. Waits, B. Morgan, M. J. Kastantin, and R. Ghodssi, "Microfabrication of 3D Silicon MEMS Structures using Gray-scale Lithography and Deep Reactive Ion Etching," Sens. Actuators A Phys. **119**(1), 245–253 (2005).
36. D.-K. Yang and S.-T. Wu, *Fundamentals of Liquid Crystal Devices*, Second Edition (John Wiley and Sons, Ltd 2014), Chap.12.
37. I.-C. Khoo, *Liquid Crystals: Physical Properties and Nonlinear Optical Phenomena* (Wiley, 1995).
38. R. D. Polak, G. P. Crawford, B. C. Kostival, J. W. Doane, and S. Zumer, "Optical determination of the saddle-splay elastic constant K24 in nematic liquid crystals," Phys. Rev. E Stat. Phys. Plasmas Fluids Relat. Interdiscip. Topics **49**(2), R978–R981 (1994).
39. G. Lippmann, "Epreuves reversibles donnant la sensation du relief," J. Phys. **7**, 821–825 (1908).
40. F. Okano, J. Arai, K. Mitani, and M. Okui, "Real-time integral imaging based on extremely high resolution video system," Proc. IEEE **94**(3), 490–501 (2006).
41. M. DaneshPanah and B. Javidi, "Profilometry and optical slicing by passive three-dimensional imaging," Opt. Lett. **34**(7), 1105–1107 (2009).
42. H. Hoshino, F. Okano, H. Isono, and I. Yuyama, "Analysis of resolution limitation of integral photography," J. Opt. Soc. Am. A **15**(8), 2059–2065 (1998).
43. X. Xiao, B. Javidi, M. Martinez-Corral, and A. Stern, "Advances in Three-Dimensional Integral Imaging: Sensing, Display, and Applications [Invited]," Appl. Opt. **52**(4), 546–560 (2013).
44. R. Martinez-Cuenca, G. Saavedra, M. Martinez-Corral, and B. Javidi, "Progress in 3-D Multiperspective Display by Integral Imaging," Proc. of IEEE Journal, Volume 97, 1067–1077, June 2009.
45. L. Yang, M. McCormick, and N. Davies, "Discussion of the optics of a new 3-D imaging system," Appl. Opt. **27**(21), 4529–4534 (1988).
46. S. N. Sinha, D. Steedly, R. Szeliski, M. Agrawala, and M. Pollefeys, "Interactive 3D architectural modeling from unordered photo collections," in ACM Transactions on Graphics (TOG), 2008, 159.

#228317 - $15.00 USD Received 20 Nov 2014; revised 9 Jan 2015; accepted 9 Jan 2015; published 15 Jan 2015

1. Introduction

Liquid crystals (LCs) have unique electro-optical characteristics that make them useful for studying and fabricating practical optical devices. There is a consensus among researchers that liquid crystal lenses can be used as an alternative to mechanically adjustable solid lens systems [1–6]. More recently, the properties of LC lenses [7–9] have received much attention. They are thin, tunable in focus, and electrically switchable to 2D/3D modes. Rather than controlling light by varying the thickness and shape of a polished material, an LC lens system tunes the refractive index of the LC by applying a voltage.

LC lenses are thus suitable for enhancing endoscope imaging systems [10], which usually have a solid lens having a few millimeters in diameter. It is advantageous to have an endoscope with smaller lens and a short focal length with 3D imaging capabilities. It is also advantageous for the device to work at low voltages (i.e., less than 20V) so that it can be used in an integrated circuit, which cannot tolerate high voltages. The advantages of 3D endoscopy are to improve the speed and accuracy of surgery. 3D imaging also helps surgeons learn to control the instrument more quickly [11]. Numerous types of LC lenses have been proposed, such as a 3D sensing system [12] a 3D imaging system [13–16], and an optical tunable LC lens [17, 18]. These systems have been investigated for research and were not in clinical use.

There are several challenges to making an improved LC lens. For instance, photo-polymerized LC lenses have short focal lengths but require high applied voltage [19] and have a complicated structure that is costly to manufacture [20]. An optical system for a 200μm aperture size based on an LC lens array has been developed but suffered from distortion. Although this can be reduced, it is impossible to extract a 3D image as a result [21]. Other LC lens systems use low applied voltage [22–25], a patterned lenticular LC lens [26–28], and a liquid lens actuated by LC pistons [29].

A careful study of the literature reveals that the liquid crystal lens array for three dimensional capturing images in particular the acquisition of medical images has not been thoroughly investigated. A clear understanding of LC lens array is very essential for taking 3D images. Therefore, the goal of this study is to develop a more rigorous understanding of LC lens array especially in an endoscope. To demonstrate the potential of this approach and its suitability for medical imaging, an array of LC lens in a hexagonal arrangement is investigated. Among the plausible explanations for these findings is that a convex-ring electrode indicates better performance compared with a flat electrode as it is shown at [30, 31]. The convex- electrodes avoid stack overflow of the electric field at the center of the lens and permit shorter focal lengths. Such electrodes make it possible to work on a wider range of applied voltages, which gives more precise control over focusing.

The primary goal of this study is to determine a convex-ring electrode not as a lens itself as it is reported in [32] but as a surrounding electrode which makes better transparency and tunability for LC lens. A large birefringence change can be achieved by a relatively small voltage such as a few volts. Focal length can vary from 2.5 cm to infinity and aperture size for each lens is 350 μm. We successfully demonstrate a hexagonal LC-lens array for capturing 3D images by using single image sensor using integral imaging. Experimental procedures, apparatus, and results are shown in following sections.

2. Convex-ring electrode fabrication

The fabrication process and operating principles of our LC lens array are schematically illustrated in Fig. 1. First, we take a glass substrate and coat it with AZ 40XT photoresist with a spin coating machine at 2000rpm for 25 seconds. This is then gently baked for 5 minutes at 60°C: see Fig. 1(a) and Fig. 5 minutes at 80°C to avoid bubbles in the resist film after photolithography using hexagonal mask see:Fig. 1(b), and finally for 7 minutes at 130°C. As the photoresist reaches the softening point, it curves [see Fig. 1(c)]. Next, we coat the AZ 40XT photoresist on the indium tin oxide (ITO, a transparent conductor) and etch the pattern

#228317 - $15.00 USD Received 20 Nov 2014; revised 9 Jan 2015; accepted 9 Jan 2015; published 15 Jan 2015

as shown in Fig. 1(e), 1(f) and 1(g).We used the Karl Suss aligner for aligning the mask. Then, a layer of the UV-curable adhesive [Norland Optical Adhesive NOA81] is added, which is a photosensitive conductive prepolymer with good optical performance over the substrate, photoresist, and ITO [see Fig. 1(c)]. Finally, we solidify this layer by polymerizing it with UV light [see Fig. 1(h)].

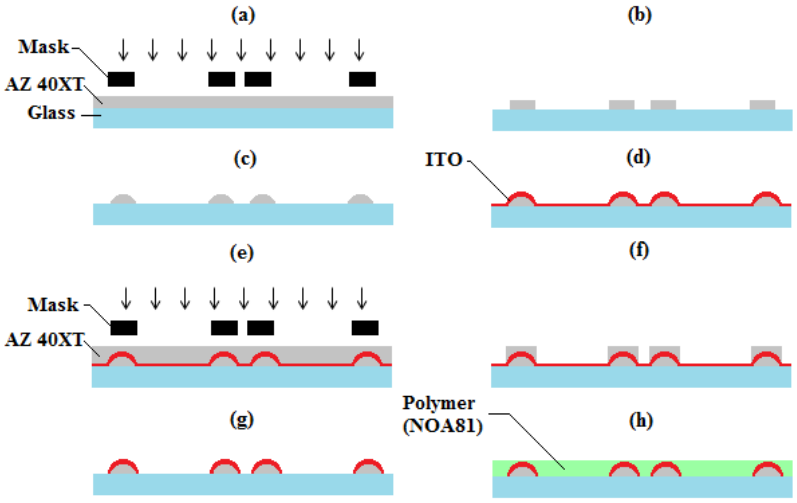

Fig. 1. Fabrication of the convex circular electrode. (a) Exposure with a UV lamp through the mask after spin-coating and soft bake, (b) Development, (c) heat treatment at 130°C (softening point), (d) 100 nm ITO is sputtered, (e) Mask alignment and exposure with a UV a lamp through the mask after spin-coating on ITO and soft bake, (f) Development, (g) Wet etching is performed, (h) Polymer (NOA81) is coated to cover the electrodes.

2.1 Device structure

Schematic of the liquid crystal is shown in Fig. 2. It consists of two layers of ITO as electrodes, one is the patterned electrode on the top and other one is as ground electrode, two glass substrates of thickness 550 µm, a 35 µm thick layer of NOA81 as an insulating layer, an LC layer with cell gap of 30 µm, and two alignment layers are coated with PVA (poly-vinyl alcohol) and mechanically rubbed for homogeneous LC alignment. The rubbing directions of the two alignment layers are antiparallel, and the lens diameter for each one is 350 µm.

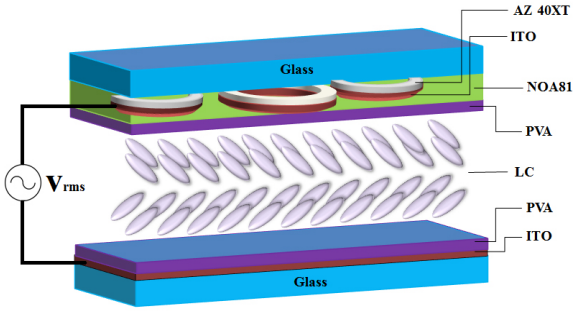

Fig. 2. Schematic of the liquid crystal (LC) lens array structure with convex-ring electrode, including a voltage source.

#228317 - $15.00 USD Received 20 Nov 2014; revised 9 Jan 2015; accepted 9 Jan 2015; published 15 Jan 2015

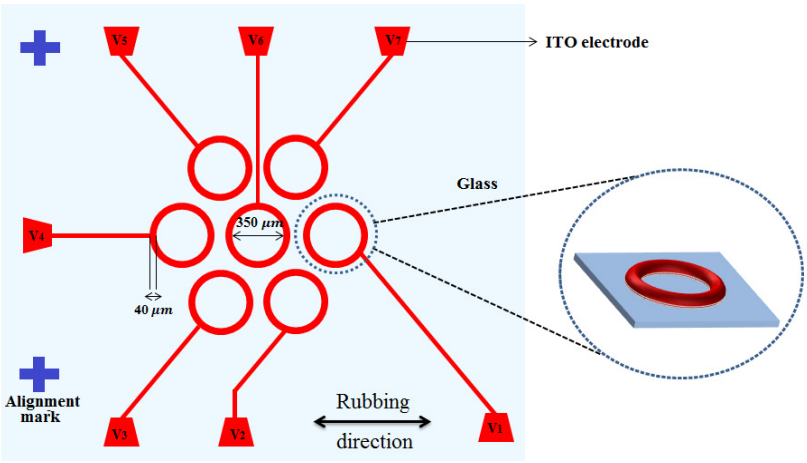

Fig. 3. Indium tin oxide (red) on a hexagonal pattern. Each lens can be applied with different voltages or same voltage.

The electrode pattern is shown in Fig. 3. Each lens can be applied with different voltages. The photo of the fabricated LC lens is shown in Fig. 4(a) and a microscopic image of the hexagonal convex curved electrodes is shown in Fig. 4(b). There are three other ways to make a curved photoresist; soft reflow process with a solvent vaporing technique [33], HBr/O2 Plasma treatment [34], and Gray-scale optical mask [35].

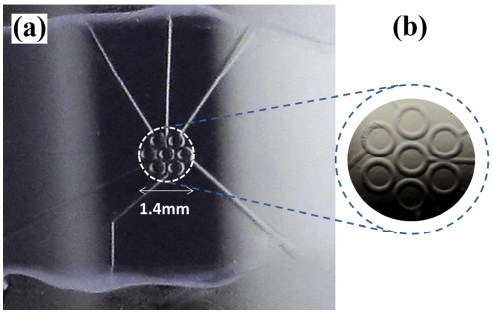

Fig. 4. (a) Photo of the fabricated Hexagonal LC micro- lens array, (b) Microscopic image of the hexagonal convex curved electrodes.

3. Convex-ring electrode for Micro LC-lens

Most LC microlenses developed thus far employ nematic LCs, which offer a large birefringence to achieve a short focal length and flat electrode which is a commonly used to approach this matter. Although this is the most comprehensive account of LC lens produced so far, it does suffer from a number of flaws. However, the main weakness of the approach is the failure to approach a short focal length. Due to a small cell gap of the liquid crystal (30μm) the electric torque will be quickly balanced by the elastic torque exerted by the surrounding LC directors. Therefore, the LC director rotation becomes stable before the LC lens can reach its minimum focal length. By changing the shape of ITO electrode to a convex-ring electrode, we can control the phase profile to approach parabolic shape thus the spherical aberration could be suppressed. To utilize the maximum intrinsic birefringence of the LC material and present the shortest possible focal length we propose a convex-electrode. We measured the focusing properties of the LC lens, the image quality, interference patterns, and focal length under different applied voltages. When a voltage (V) is applied to the electrodes, the LC layer experiences an inhomogeneous electric field because the top ITO electrode is

#228317 - $15.00 USD Received 20 Nov 2014; revised 9 Jan 2015; accepted 9 Jan 2015; published 15 Jan 2015

hole-like. When a voltage is applied, the convex- ring electrode makes a gradient electric field distribution in the LC layer. The electric field is the largest at the center of electrode and is smallest at the edge of the electrode. The direction of the LC directors from near the edge of the convex-ring electrode to the center of the lens varies more smoothly than the flat-electrode does.

In many liquid crystal devices, the liquid crystal director configuration cannot be calculated analytically and must be numerically computed. Under a given external field and boundary condition, when a liquid crystal is in the equilibrium state, the total free energy is minimized. If the system is initially not in the equilibrium state, it will relax into a state with lower free energy. As the liquid crystal director configuration evolves, the free energy decreases. The change of the director configuration stops when the minimum free energy is reached. The dynamic equation for the change of the liquid crystal director can be used to numerically calculate the equilibrium director configuration, which is referred to as the relaxation method. A liquid crystal medium prefers a uniform director distribution. A variation of the director in space induces an increase of the free energy. According to the elastic theory for liquid crystals, the elastic energy related to the variation of the director 'n' in space can be written as

$$f_{elastic} = \frac{1}{2}k_{11}(\nabla \cdot n)^2 + \frac{1}{2}k_{22}(n \cdot \nabla \times n)^2 + \frac{1}{2}k_{33}(n \times \nabla \times n)^2 \quad (1)$$

This equation is known as the Oseen-Frank distortion energy. The liquid crystal director n can be specified by its three components $\mathrm{n} = (\mathrm{n_x}, \mathrm{n_y}, \mathrm{n_z})$, with the three elastic constants $\mathrm{k_{11}}$, $\mathrm{k_{22}}$ and $\mathrm{k_{33}}$. The three terms in the equation are related to deformations due to splay, twist and bend respectively. The effect of an electric field when voltage is applied to ITO electrodes can be described using a free energy density term which is related to the interaction of the applied electric field and the director of the liquid crystal molecule.

$$f_{electric} = -\frac{1}{2}[\varepsilon_{\perp}E^2 + \Delta\varepsilon(n \cdot E)^2] \quad (2)$$

The total free energy of the nematic LC directors in the presence of the static electric field can be written as [36, 37]:

$$F_{total} = f_{elastic} + f_{electric} =$$
$$\frac{1}{2}k_{11}(\nabla \cdot n)^2 + \frac{1}{2}k_{22}(n \cdot \nabla \times n)^2 + \frac{1}{2}k_{33}(n \times \nabla \times n)^2 - \frac{1}{2}[\varepsilon_{\perp}E^2 + \Delta\varepsilon(n \cdot E)^2] \quad (3)$$

The simulated director configuration using commercial software 2DiMOS is shown in Fig. 5 for a flat and convex-ring electrode. The parameters of the nematic mixture E7 used for simulation are: $\mathrm{k_{11}} / \mathrm{k_{33}} = 1.54$, $\mathrm{k_{22}} / \mathrm{k_{11}} = 0.93$;for $\lambda_0 = 435\mathrm{nm}$, $n_e = 1.8208$ and $n_o = 1.544$ [38] The rubbing directions were arranged to be anti-parallel (~2 degrees) and the two slides were separated with 30 μm thick spacers. The voltage applied across the LC cell is $\mathrm{V_{rms}} = 5\mathrm{V}$. A gap between the patterned-electrode and liquid crystal layer is necessary not only to avoid confining the gradient field around the edge of the patterned electrode but also to allow electric field distributes to the center of the lens to make an LC cell works like a lens. Due to this NOA81 layer from the top glass substrate to the LC layer is required. Figure 6 shows the experimental setup we used to probe the voltage-dependent focal length of the lens.

#228317 - $15.00 USD Received 20 Nov 2014; revised 9 Jan 2015; accepted 9 Jan 2015; published 15 Jan 2015

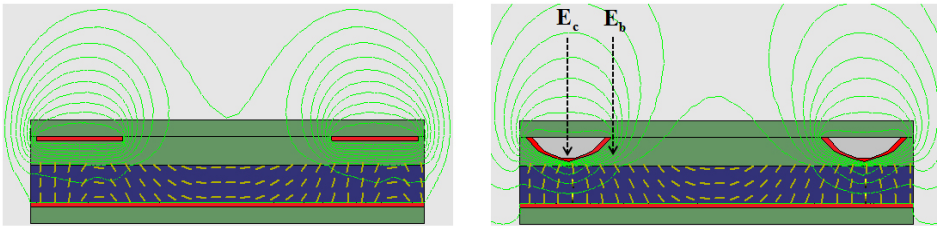

Fig. 5. Simulated results for the same applied voltage, An LC using a flat electrode (left) and convex-ring electrode (right).

It is noted that ITO electrode is not used as a lens itself and the lens forms between the convex-ring electrodes. The convex- ring electrode differs from flat electrode in a number of important ways. This can be which permits to have smaller inactive areas. Furthermore, experimental results show more homogeneous and symmetrical field surrounding convex-ring electrode compared to a flat electrode. Therefore, the lens has less distortion as well. Within the LC layer, the electric field at the border of electrode E_b and the electric field at the center of electrode E_c [see Fig. 5 (right)] can be calculated as follows:

$$E_b = \frac{\frac{V}{\varepsilon_{lc}}}{(\frac{d_{lc}}{\varepsilon_{lc}} + \frac{d_{ins}}{\varepsilon_{ins}})} \tag{4}$$

$$E_c = \frac{V}{d_{lc}} \tag{5}$$

The device was filled with nematic LC material E7 (Merck) with the following properties: extraordinary and ordinary dielectric constants $\varepsilon_p = 19.0$ and $\varepsilon_s = 5.2$ of the LC, respectively, and the birefringence refractive index of the LC, Δn, is 0.225. The effective dielectric constant of the LC, ε_{lc}, is 9.74. The LC and glass layers (d_{lc} and d_g) are 30 μm and 550 μm thick, respectively. The glass dielectric constant $\varepsilon_g = 7.75$, the dielectric constant of NOA81 $\varepsilon_{ins} \sim 5$ at a frequency of 1 kHz, and the insulator thickness d_{ins} is 35 μm. Substituting the values into Eq. (4) and Eq. (5) [36] gives $E_c = 33.33V$ V/μm and $E_b = 10.18V$ V/μm. Although the electric field is lower at the border than at the center, which practically reduces the electric field gradient from the center to the border.

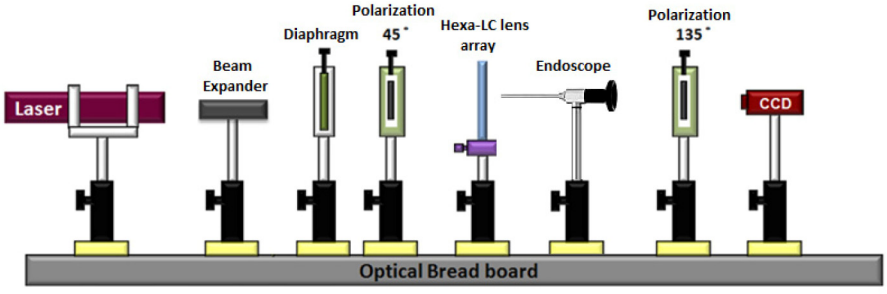

Fig. 6. Experimental setup for 3D endoscopy using Hexagonal LC lens array.

#228317 - $15.00 USD Received 20 Nov 2014; revised 9 Jan 2015; accepted 9 Jan 2015; published 15 Jan 2015

Based on the measured interference fringes at different voltages, the focal length of the lens cell can be calculated using the equation $f_{lc}(V)=\pi D^2/4\lambda\Delta\delta$, where D is aperture width of the lens, λ is the wavelength of incident laser beam, and $\Delta\delta$ is the phase difference between the central region and the border region of the aperture in the interference patterns [5]. The total focal length of the LC lens can then be expressed as following, where $f_{ins}(V)$ is the fixed focal length of the Insulating layer (NAO81).

$$\frac{1}{f(V)}=\frac{1}{f_{lc}(V)}+\frac{1}{f_{ins}(V)} \tag{6}$$

Figure7 shows the comparison of flat electrode and convex-ring electrode It can been seen that the flat electrode has a very short range of focal length variation. The focal length varies as voltage changes from 1 volt to 2.2 volts and after which there is no variation and the focal length stays the same value. The convex-ring electrode has a wider range of variation compare with flat electrode. The focal length can change as voltage changes from 1 volt to 3.9 volts. This is not the only advantage of this type of lens. This specific convex-ring electrode design can lower the focal length up to 2.5 cm which is impossible for the flat electrode to achieve.

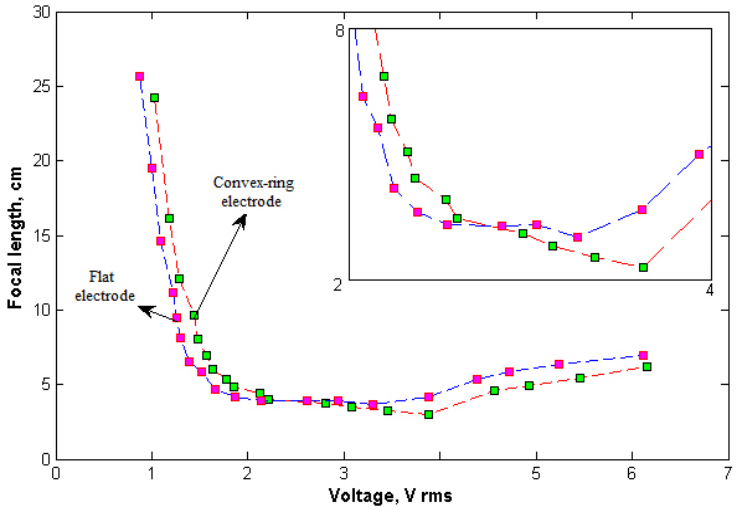

Fig. 7. Focal length variation vs. voltage for flat electrode (pink squares) and convex-ring electrode (green squares).

The phase retardation was changed when liquid crystals were rotated by applying a voltage to the convex-ring electrodes. Phase retardation of an LC lens is given by:

$$\varphi=2\pi d_{lc}\frac{\Delta n}{\lambda} \tag{7}$$

where λ is the wavelength, $\Delta n=0.225$, $d_{lc}=30\,\mu m$ and $\lambda=632nm$. Therefore, the maximum phase difference is $\Delta\varphi=10\times 2\pi$ which means we can observe 10 rings. To evaluate the optical properties of this hexagonal LC lens array, we recorded the interference fringes between the ordinary and extraordinary rays that is, rays polarized perpendicular and parallel to the plane of incidence, respectively using a helium-neon (He-Ne) laser beam (λ = 632 nm) that passes through the LC lens placed between two crossed polarizers. Figure 8 shows the recorded interference fringes at various applied voltages. When the voltage is applied, the appearance of the interference fringes changes as the LC directors reorients themselves in the applied

#228317 - $15.00 USD Received 20 Nov 2014; revised 9 Jan 2015; accepted 9 Jan 2015; published 15 Jan 2015

electric field. The retardation difference of two adjacent constructive or destructive interference rings indicates a phase change of 2π, and the variation in phase retardation induced by the applied voltage shows how the electrical field alters the lens properties.

A liquid crystal lens can produce a phase shift across the incident beam by electrically tuning the refractive index. The phase difference between each constructive interference ring based on their positions is marked. Therefore, if we count the interference rings in direction of the rubbing direction from the edge of ITO electrode toward the center of the LC lens we can define the phase variation in different positions according to cumulative phases in each ring. This means that phase difference increases from the edge toward the center of the LC lens. A trend line through a set of data is plotted in Fig. 9. Solid curves are the fitting curves at various values of Vrms.

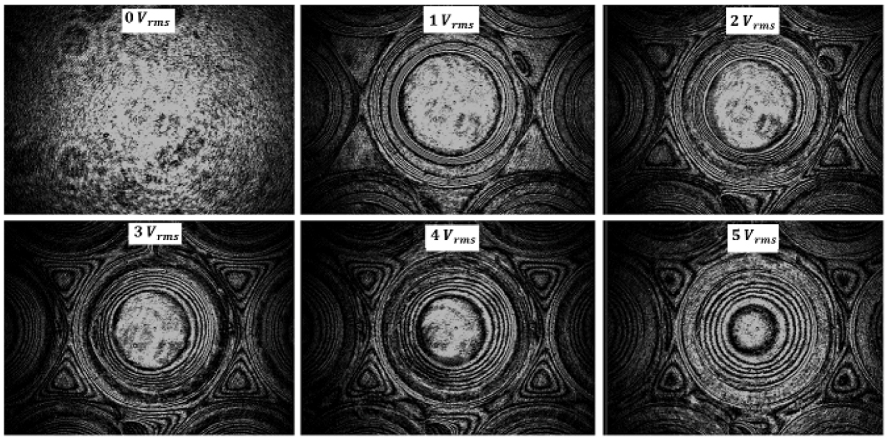

Fig. 8. Interference patterns for proposed LC lens.

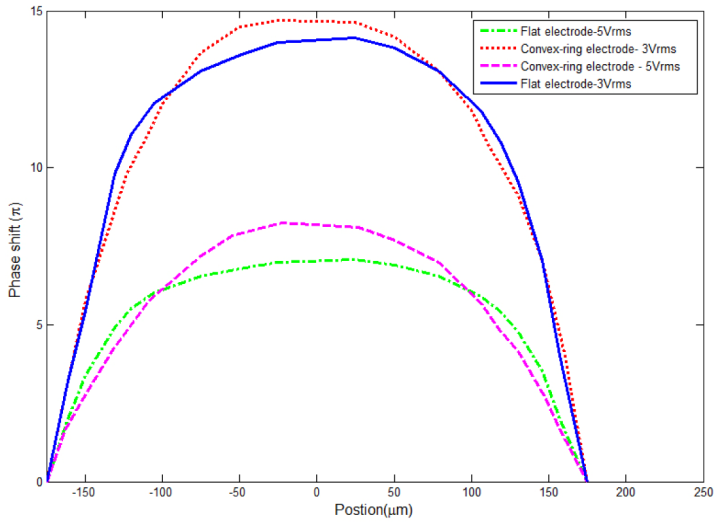

Fig. 9. Phase shift profiles comparison for flat-electrode and convex-ring electrode with different applied voltages.

It shows that the fabricated convex-ring electrode LC lens not only has a better performance as a micro-lens, but it also has the potential of being able to lower focal length in the proposed 2D/3D endoscope. For flat electrode in the high voltage regime above 5 V, because a bell-shaped distribution for the LC phase profile is not produced therefore no lens

#228317 - $15.00 USD Received 20 Nov 2014; revised 9 Jan 2015; accepted 9 Jan 2015; published 15 Jan 2015

effect exists. However the phase profile of the incident plane light wave polarized for convex-ring electrode is more similar to bell-like phase profile.

4. 3D Optical imaging using LC lens endoscope

Current research indicates that there are three reasons a 3D endoscope will improve the speed of surgery. These are 1) the average time to complete a suturing task in 3D imaging is shorter than 2D; 2) 3D imaging provides greater precision with significantly lower error rates in grasping tasks; and 3) 3D imaging reduces training time for new surgeons [11]. We use an integral imaging system [39–45] to capture the elemental images, that is, the perspective images of the object formed by each LC lens[see Figs. 6 and 10].

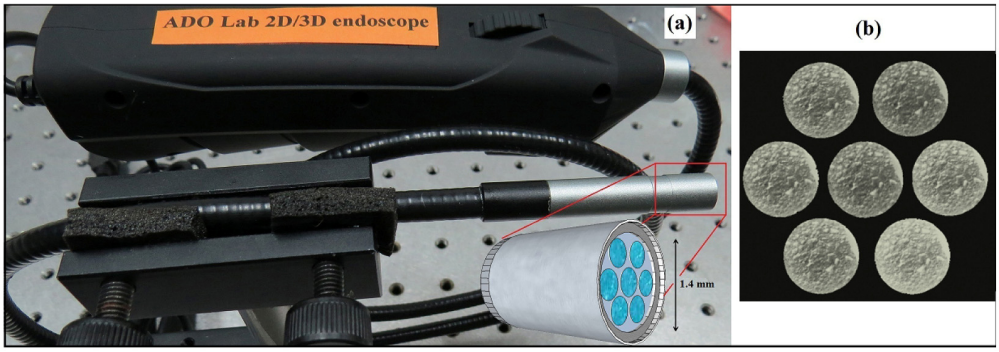

Fig. 10. (a) An endoscope with the embedded hexagonal convex-ring electrode LC lens placed in front of the endoscope, (b) captured image in each LC lens.

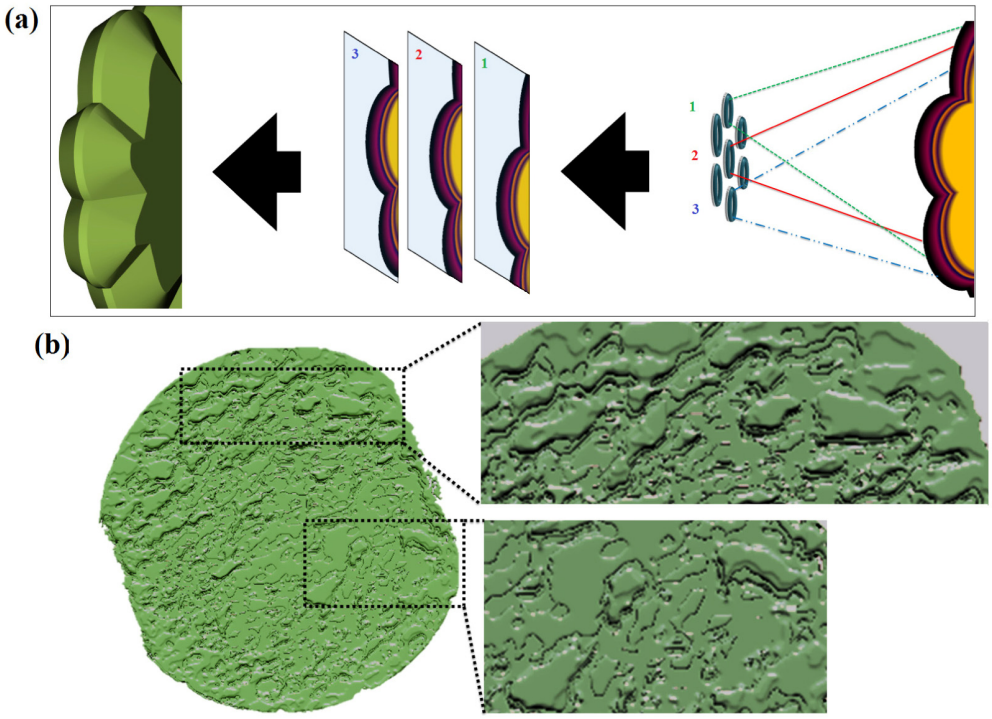

Fig. 11. (a) Schematic of reconstructing a 3D image from 2D images obtained by LC lens array. (b) 3D image extracted from 2D elemental image array captured by the hexagonal LC - lens array and the endoscope.

#228317 - $15.00 USD Received 20 Nov 2014; revised 9 Jan 2015; accepted 9 Jan 2015; published 15 Jan 2015

The focal length of the convex-ring electrode LC lens array can be electrically varied by changing the effective refractive index of the LC region in each lens independently. Therefore we can implement 3-D imaging without moving the image sensor or the CCD sensor of endoscope. The LC lens can focus on the various depths or slices of the 3D object as the applied voltage varies. The sectional 2D images of under study can obtained at arbitrary depth positions by changing the focal length of the convex-ring electrode LC lens array for each lens. 3D image data may be constructed by capturing multiple 2D images of the 3D object and extracting the depth information according to various approaches [44, 46]. In our experiments, each lens can capture a 2D perspective image of the 3D scene from different viewing angles at tunable depths as shown in Fig. 10. Thus, the system can record the depth-sampled image by properly synchronizing the 2D image to be captured by varying the focal length, as it shown in Fig. 11(a). 3D image data is reconstructed using several 2D images captured by LC lens. We investigated the imaging properties of this LC lens when it was placed 2 mm from the objective lens of a side-view endoscope with a $20 \times 25\,\mathrm{mm}^2$ test object a sponge placed 73 mm from the LC lens. Figure 10(a) demonstrates a convex-ring electrode LC lens array that is mounted to a front view endoscope. We took images of the test object as shown in Fig. 10(b). We captured images of an object from different viewing angles and processed them using integral imaging to reconstruct the 3D image of the object. Figure 11(b) is a reconstructed 3D image using the seven elemental images taken using the hexagonal convex-ring electrode LC lens array.

5. Conclusion

Conventional 3D endoscopes consist of two lenses and two sensors, which enlarged the size of the instrument and have limitations imposed by stereo systems. We have successfully developed a hexagonal LC-lens array for capturing 3D images by using a single sensor using integral imaging. The diameter of developed 3D endoscope is less than 1.4mm, which is close to conventional 2D endoscope. Another significant finding from this study is that we propose convex-ring electrode to produces parabolic-like electric field distribution, thus lowering the focal length to less than 2.5 cm. which enables the endoscope to capture closer objects for medical applications. Finally, a hexagonal convex-ring electrode LC lens array with single senor endoscope for 2D/3D switching and easy mounting is successfully demonstrated.

#228317 - $15.00 USD Received 20 Nov 2014; revised 9 Jan 2015; accepted 9 Jan 2015; published 15 Jan 2015